ORIGINAL RESEARCH

A.L. Wentland
O. Wieben
F.R. Korosec
V.M. Haughton

Accuracy and Reproducibility of Phase-Contrast MR Imaging Measurements for CSF Flow

BACKGROUND AND PURPOSE: PCMR, widely used for the evaluation of blood flow, has been adopted for the assessment of cerebrospinal fluid flow in a variety of disorders. The purpose of this study was to evaluate the accuracy and reproducibility of 2 fast PCMR techniques for measuring CSF flow.

MATERIALS AND METHODS: Velocities were calculated from RPC and CPC images of fluid flowing in a tube at a constant velocity. Error and the COV were computed for average and peak velocities. Additionally, measurements of sinusoidally fluctuating flow and of CSF flow in 5 healthy volunteers were acquired with the RPC and CPC acquisitions.

RESULTS: For constant velocity experiments, error for the RPC and CPC acquisitions averaged +1.15% and +8.91% and COVs averaged 1.29% and 3.01%, respectively. For peak velocities of ≥12.6 cm/s, error with RPC or CPC ranged from −33.3% to −36.9% and COVs were 0%–4% for RPC and 1%–7% for CPC. For peak velocities of ≤6.4 cm/s, RPC and CPC overestimated velocity by >250%. For fluctuating flow, both acquisitions showed similar flow patterns. In volunteer studies, peak systolic and diastolic velocities were not significantly different.

CONCLUSIONS: The RPC and CPC sequences measure velocities on the order of CSF flow with an average error of ≥9%. The 2 techniques significantly overestimate peak velocities <6.4 cm/s, with maximum errors of 209% and 276% and maximum COVs of 100% and 73% for the RPC and CPC sequences, respectively. Measurements of CSF velocities in human volunteers and of sinusoidally fluctuating phantom velocities did not differ significantly between the 2 techniques.

ABBREVIATIONS: COV = coefficient of variation; CPC = Cartesian-based phase contrast; PCMR = phase-contrast MR imaging; QA = quality assurance; RBW = receiver bandwidth; RPC = radially sampled phase contrast; SNR = signal intensity–to-noise ratio; VENC = velocity encoding; vps = views per segment

PCMR, widely used for the evaluation of blood flow,[1] has been adopted for the assessment of CSF flow in a variety of disorders, including Chiari I malformation and syringomyelia.[2-8] The conventional nonsegmented cardiac-gated PCMR sequence for measuring blood flow has been modified to reduce acquisition time to facilitate the acquisition of images at multiple levels or during a breath-hold. This work seeks to validate 2 approaches for cine CSF imaging within <30 seconds: 1) a rectilinearly acquired CPC acquisition, and 2) an undersampled RPC acquisition.[9]

Compared with the velocities in blood-flow imaging (50–300 cm/s), the peak velocities of interest in the imaging of CSF flow are <20 cm/s and commonly on the order of 1–2 cm/s.[10] For slower flow, bipolar gradients are adjusted to achieve a lower VENC value by means of TE and TR times. An increase in the magnitude of the gradient may introduce errors due to stronger eddy currents. Because of these potential errors, the accuracy of the acquisition for the measurement of low velocities must be validated.

The acquisition time of CPC is shortened to approximately 30 seconds by incorporating data segmentation into a conventional cardiac-gated Fourier-encoded sampling scheme.[11] While this approach reduces scan time, the segmentation also reduces temporal resolution within the cardiac cycle. In this acquisition, 1 segment, consisting of several phase-encoding lines of *k*-space data, is acquired repeatedly throughout the cardiac cycle to provide information from multiple cardiac phases. In each subsequent heartbeat, another *k*-space segment is acquired until all of the desired *k*-space is sampled. The number of cardiac phases is determined by the heart rate (R-R interval), the number of vps, the TR, and the number of flow directions sampled. Such CPC sequences, which are available on most clinical MR imaging systems, have been validated[12] and are routinely used for vascular applications. While the segmented CPC method has been used for rapid PCMR measurements of CSF flow[13] and for relating CSF flow to pressure,[14] no validation of its accuracy and precision has been reported, to our knowledge.

With the RPC method, *k*-space is sampled as a series of radial projections, each traversing through the center of *k*-space.[9,15] Spatial resolution is determined by the sample spacing along each radial projection. Reducing the number of radial projections neither diminishes spatial resolution nor causes wrap-around artifacts. In certain imaging applications, a high SNR can be achieved even if the number of acquired projections is significantly less than the number of projections

Received September 30, 2009; accepted after revision December 18.

From the Departments of Radiology (A.L.W., O.W., F.R.K., V.M.H.) and Medical Physics (A.L.W., O.W., F.R.K.), University of Wisconsin School of Medicine and Public Health, Madison, Wisconsin.

V.M.H. was supported by a Center of Excellence grant from the Norwegian Research Council to the Center for Biomedical Computing at Simula Research Laboratory.

Paper previously presented at: Annual Meeting of the American Society of Neuroradiology, May 6–12, 2006; San Diego, California.

Please address correspondence to Andrew L. Wentland, BS, Departments of Radiology and Medical Physics, Wisconsin Institutes for Medical Research, 1111 Highland Ave, 1310J, Madison, WI 53705; e-mail: alwentland@wisc.edu

DOI 10.3174/ajnr.A2039

required to fulfill the Nyquist sampling criterion. Therefore, the RPC acquisition allows higher spatial resolution per unit time than that achievable with spin-warp encoding methods.[9,15] However, radial undersampling may reduce SNR and produce streak artifacts. Radial undersampling factors of ≤12 with good accuracy have been recently reported in a validation study for renal artery flow.[15]

The goal of this study was to measure the accuracy and reproducibility of average and peak velocity measurements acquired from the 2 phase-contrast methods over the range of CSF velocities found in the foramen magnum, which is, in most cases, from 2 to 20 cm/s.[16]

Materials and Methods

Construction of the Flow Phantom

A flow phantom was constructed by connecting polyethylene tubing to a computer-controlled pump, 100060 UHDC Flow System (RG Shelley, Toronto, Ontario, Canada), which pumps fluid at a preset flow rate with an accuracy of ±1%, as determined by the pump manufacturer. The pump was programmed to deliver temporally constant or sinusoidally varying flow rates. The tubing had a length of 8 m to allow pump placement outside the MR imaging scanner room. The tubing was placed in the scanner bore so that 2 straight segments with opposing flow directions were parallel to the z-axis of the scanner with a U-shaped section at the end of the bore (Fig 1). A cubic MR imaging QA phantom was added for additional coil loading. The cubic MR imaging QA phantom and the tubing of the flow phantom were situated in the center of a standard quadrature birdcage head coil of a clinical 1.5T MR imaging scanner (Fig 1) with high-performance gradients (Signa HDx; GE Healthcare, Waukesha, Wisconsin). For constant velocities of <0.8 cm/s, gadolinium-doped fluid (density = 1.02 g/cm^3, viscosity = 4.1 mPa·s) was pumped through tubing with an inner diameter of 12.7 mm. Due to a change in protocol, for constant velocities >8 cm/s, fluid was pumped through tubing with an inner diameter of 6.4 mm. Fluid was also pumped at a velocity that varied in a sinusoidal manner at an average velocity of 3.1 cm/s (peak Reynolds number = 98.7 and assumed to be laminar).

The setup of the U-shaped region and the analyzed tubing region was designed so that the imaging plane had fully developed laminar flow as determined by the minimum distance for the entry length. For the straight segment of the tubing, entry length is defined as $l_s = 0.25 \cdot a \cdot Re$, where a is the radius of the tubing and Re is the Reynolds number.[17] In our study, the required entry length was 15.7 cm, which was significantly exceeded in the phantom setup (Fig 1).

Phantom Studies: Constant Flow

Images were obtained in an axial orientation perpendicular to the tubing and through the center of the phantom by using both the RPC and CPC methods. Multiple images, or phases, were generated through a simulated 1-second cardiac cycle. Scans were triggered with a waveform generator, M310 ECG Simulator (Fogg System, Denver, Colorado), at 60 cycles per minute.

To generate velocities >8 cm/s, the flow pump was set to flow rates of 2.0, 4.0, 6.0, or 8.0 mL/s, and scans were acquired 3 times with both of the sequences for each of the specified flow rates. The VENC value was adjusted to 16, 32, 48, and 64 cm/s for the 4 flow rates, respectively, to optimize the SNR for images acquired at each velocity. The actual average velocity was calculated as the flow rates divided by the cross-sectional area (0.317 cm^2) of the tubing. Actual average velocities for flow rates of 2.0, 4.0, 6.0, and 8.0 mL/s were 6.3, 12.6, 19.0, and 25.3 cm/s, respectively. Assuming laminar flow, the actual peak velocities in the tubing were calculated as the average velocities multiplied by 2. Actual peak velocities for the set flow rates were 12.6, 25.2, 38.0, and 50.6 cm/s, respectively. For scans acquired with velocities <8 cm/s, the flow pump was set to flow rates of 1.0, 2.0, and 4.0 mL/s. For all scans with velocities of <8 cm/s, the VENC was set to 10 cm/s, as is standard in our clinical examinations. Actual average velocities for flow rates of 1.0, 2.0, and 4.0 mL/s were 0.8, 1.6, and 3.2 cm/s, respectively. Actual peak velocities for these flow rates were 1.6, 3.2, and 6.4 cm/s, respectively.

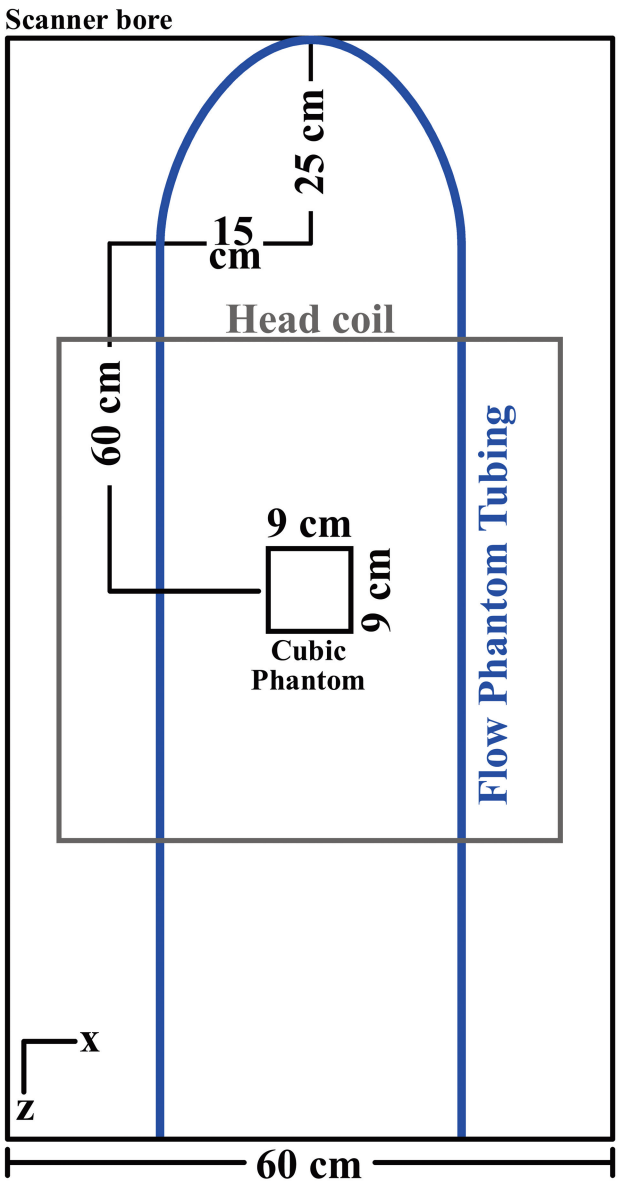

Fig 1. Diagram of the setup used in phantom studies for evaluating CPC and RPC. Tubing was connected to a computer-controlled flow pump. The tubing was looped around a cubic MR imaging QA phantom and situated in the horizontal plane of the scanner along the z-axis.

RPC images were obtained with the following parameters: flip angle = 30°, number of signal averages = 1, TR = 10.8–13.5 ms depending on the VENC, TE = 3.7–4.6 ms depending on the VENC, RBW = ± 31.25 kHz, FOV = 24 cm, section thickness = 5 mm, flow encoding in the superior/inferior direction, number of projections =

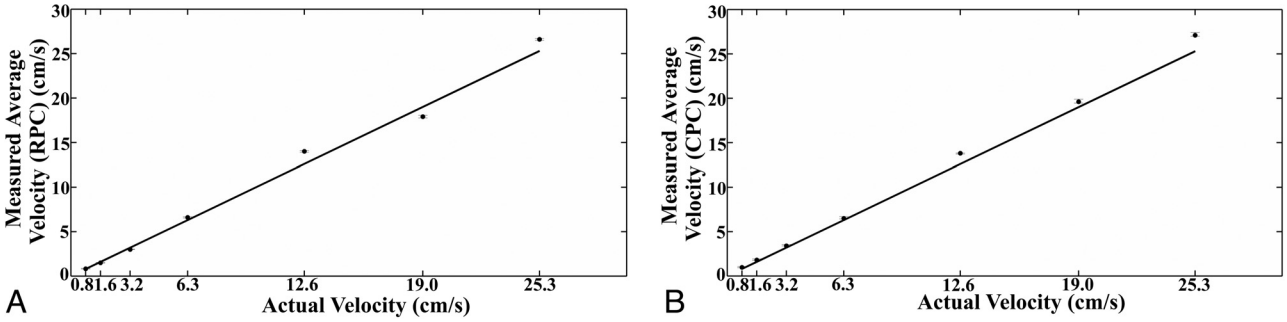

Fig 2. Average measurements of constant velocities obtained with the RPC (*A*) and CPC (*B*) acquisitions compared with actual velocities. The solid line represents unity. Error bars are SDs.

64, vps = 2, sample points along the readout direction = 256, number of cardiac phases = 20–25 depending on the VENC, prospective gating, and flow compensation and cardiac gating enabled. The CPC images were acquired with identical parameters except for the following differences: TR = 6.7–8.5 ms depending on the VENC, TE = 3.2–4.9 ms depending on the VENC, phase-encoding values = 128, FOV = 24 × 12 cm^2, retrospective gating, and 14–20 cardiac phases. With the above parameters, the scanning time for both acquisitions was 34 seconds for a heart rate of 60 beats per minute. The chosen VENC ranged from 10 to 64 cm/s depending on the flow rate selected.

Average and peak velocities were calculated from the RPC and CPC images with a commercial flow analysis package, CV Flow (Medis, Leiden, the Netherlands). A region of interest was drawn to encompass the lumen of the tubing on a magnitude image, and the region of interest was copied to the phase images across the cardiac cycle by the software. The average velocity across cardiac phases was calculated for the region of interest. The software also provided the peak velocity in each region of interest, in other words, from the greatest velocity as measured from a single voxel.

As a measure of accuracy, error was calculated as the difference between the average measured velocity and the known velocity (as calculated from the pump setting) normalized to the known velocity:

$$error = \frac{x_{ave}/x_k}{x_k}$$

where x_{ave} is the average measured values of velocity and x_k is the known velocity. As a measure of precision, COV was computed as SD divided by the mean.

Phantom Studies: Sinusoidal Flow

The velocity rate was also set to vary sinusoidally with an average velocity of 3.1 cm/s, a periodicity of 1 second, and a peak-to-peak amplitude of 6.2 cm/s to test the lower limit of flow measurements short of retrograde motion. The sinusoidally varying flow in the phantom was imaged with RPC and CPC and parameters identical to those used to image the constant flow in the phantom. The VENC was set at 10 cm/s for both acquisition methods. The scans were obtained 3 times with each scanning technique. Velocities calculated from the flow analysis package were recorded for each phase of sinusoidal flow and were plotted as a function of trigger delay. The data were compared to a sinusoid of the form $a + b \times sin[2\pi(t - t_0)]$, and the root mean square differences between the measurements and fit curves were computed. The measured peak velocities at the zenith and nadir of the sinusoidal waveform were similarly calculated and tabulated. The average absolute differences between measurements for the 2 acquisitions were computed and tested for statistical significance with a Student *t* test.

Volunteer Studies

Scans were obtained with the RPC and CPC acquisitions on 5 volunteers (1 man, 4 women; mean age, 32 ± 12 years) with the written consent of the volunteers. Institutional review board approval for this prospective study was obtained according to our institutional guidelines. Data were handled to comply with Health Insurance Portability and Accountability Act standards. Sections were prescribed at the level of the foramen magnum, defined in sagittal images by the tip of the clivus anteriorly and of the occipital bone posteriorly. RPC scans were acquired with the following parameters: flip angle = 30°, NEX = 1, TR/TE = 6.0/3.0 ms, RBW = ± 31.25 kHz, FOV = 24 cm, section thickness = 5 mm, flow encoding in the superior/inferior direction, number of projections = 64, vps = 2, sample points along the readout direction = 256, number of cardiac phases = 23, prospective gating, and flow compensation and cardiac gating enabled. CPC scans were acquired with identical parameters except for the following differences: TR/TE = 11.2/5.6 ms, phase-encoding values = 128, ½ FOV, retrospective gating, and 14 cardiac phases. Acquisition times for the RPC and CPC acquisitions ranged from 24 to 30 seconds, depending on the length of time required to scan more than 32 heartbeats. The VENC was set at 10 cm/s.

Image quality and artifacts were assessed by a neuroradiologist familiar with CSF flow imaging. Velocities measured from a volunteer were plotted as a function of trigger delay for both acquisitions. Peak craniad (systolic) and caudad (diastolic) CSF velocities, that is, the largest positive and negative velocities in any region of interest, were tabulated for both acquisitions for all volunteers. The average absolute differences between measurements for the 2 acquisitions in both systole and diastole were computed and tested for statistical significance with a Student *t* test.

Results

Phantom Studies: Constant Flow

Both the RPC and CPC acquisitions demonstrated good image quality of the phantom and the tubing, with a spatial resolution of 0.5 mm. RPC images demonstrated marked streak artifacts away from the lumen of the tubing. Mild phase ghosting was apparent in images obtained with the CPC acquisition but not with the RPC acquisition.

For the actual average velocities of 0.8, 1.6, 3.2, 6.3, 12.6, 19.0, and 25.3 cm/s, the velocities calculated by using the RPC

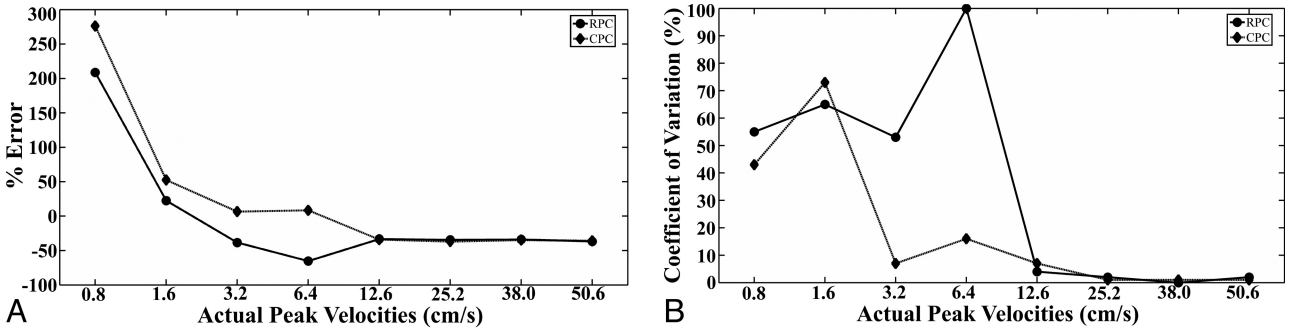

Fig 3. Error (*A*) and coefficient of variation (*B*) of peak velocity measurements in a constant flow phantom calculated from the RPC and CPC acquisitions. Actual peak velocities ranged from 0.8 to 50.6 cm/s.

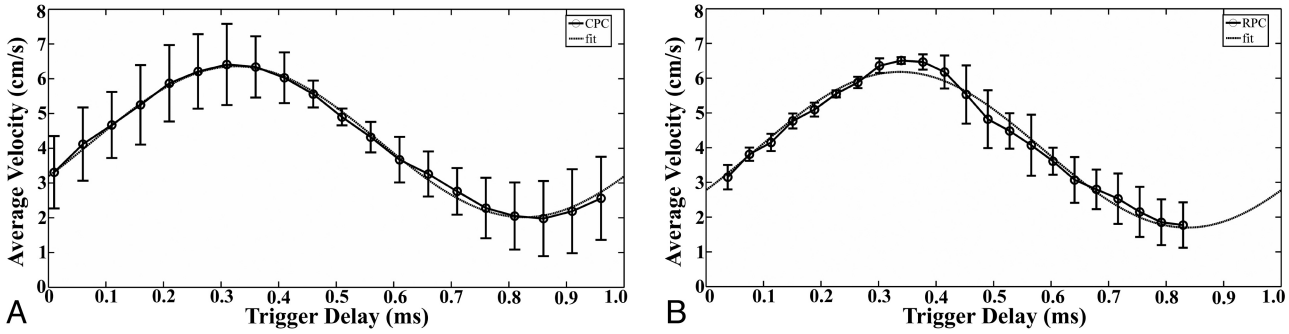

Fig 4. Velocity (± SD) calculated from the CPC (*A*) and RPC (*B*) acquisition data plotted as a function of time for a sinusoidal flow rate of 1 mL/s at 60 beats per minute. The RPC data were acquired with 64 projections and 2 vps. The CPC data were acquired with 128 phase-encoding values and a ½ FOV. Three scans were obtained with each acquisition and error bars are shown. For each set of data, a sinusoidal curve of the form $a + b \times sin[2\pi(t - t_0)]$ was fitted.

images and averaged from 3 experiments were 0.83 ± 0.04, 1.5 ± 0.04, 3.0 ± 0.02, 6.6 ± 0.07, 14.0 ± 0.09, 17.9 ± 0.15, and 26.6 ± 0.11 cm/s, respectively (Fig 2*A*). Similarly, the velocities calculated by using the CPC images and averaged from 3 experiments were 0.97 ± 0.09, 1.8 ± 0.12, 3.4 ± 0.14, 6.5 ± 0.19, 13.8 ± 0.02, 19.6 ± 0.28, and 27.1 ± 0.31 cm/s, respectively (Fig *2B*). Error for the RPC velocity measurements ranged from −5.8% to 11% (average = 1.15%) and for CPC varied from 3.2% to 21% (average = 8.91%). COVs for RPC varied from 0.3% to 3.9% (average = 1.29%) and, for CPC, varied from 0.1% to 7.6% (average = 3.01%). Errors for the CPC velocity measurements were largest for the 2 slowest velocities. The COVs were the greatest for the slowest velocity in both the RPC and CPC acquisition measurements.

When measuring peak velocities, error and the COV tended to decrease as velocities increased (Fig 3). Error for peak velocities measured with RPC or CPC ranged from −33.3% to −36.9% when the velocity was ≥12.6 cm/s (Fig 3). For peak velocities <12.6 cm/s, error in some cases exceeded 250% while the COVs in some cases reached 100% for measurements acquired with the RPC and CPC methods.

Phantom Studies: Sinusoidal Flow

For sinusoidal flow measurements, average velocities measured by using images obtained with the RPC and CPC acquisitions ranged from 1.8 to 6.5 cm/s and approximated a sinusoidal waveform (Fig 4). For the RPC and CPC acquisitions, the root-mean-square differences between average velocity measurements and the sinusoidal fit were 0.19 and 0.10, respectively (Fig 4). The RPC acquisition had a greater number of cardiac phases across the simulated R-R interval (22 phases) than did the CPC acquisition (20 phases) but did not cover as much of the simulated R-R interval as did the CPC acquisition (Fig 4). Note that the RPC acquisition was prospectively gated, whereas the CPC acquisition was retrospectively gated. The average velocity at the zenith of the sinusoidal waveform for the RPC images was 6.5 ± 0.1 cm/s and 6.4 ± 1.2 cm/s for the CPC images (Table 1). The average velocity at the nadir of the sinusoidal waveform for the RPC images was 1.8 ± 0.7 cm/s and for the CPC images was 2.0 ± 1.1 cm/s (Table 1). The peak velocity recorded at the zenith was 11.5 ± 0.6 cm/s for the RPC images and 10.2 ± 0.9 cm/s for the CPC images. The peak velocity recorded at the nadir was 4.3 ± 0.4 cm/s for the RPC images and 5.0 ± 0.6 cm/s for the CPC images (Table 1). The average absolute difference between average velocities and peak velocities measured with the 2 methods was 0.6 ± 0.6 cm/s, a difference that was not significant statistically ($P = .79$).

Table 1: Average and peak velocities at the zenith and nadir of a sinusoidal waveform measured in a phantom with the RPC and CPC acquisitions

	RPC[a]	CPC[a]	Absolute Difference
Average velocity at zenith (cm/s)	6.5 ± 0.1	6.4 ± 1.2	0.1
Average velocity at nadir (cm/s)	1.8 ± 0.7	2.0 ± 1.1	0.2
Peak velocity at zenith (cm/s)	11.5 ± 0.6	10.2 ± 0.9	1.3
Peak velocity at nadir (cm/s)	4.3 ± 0.4	5.0 ± 0.6	0.7
Average			0.6 ± 0.6

[a] Mean values ± SDs.

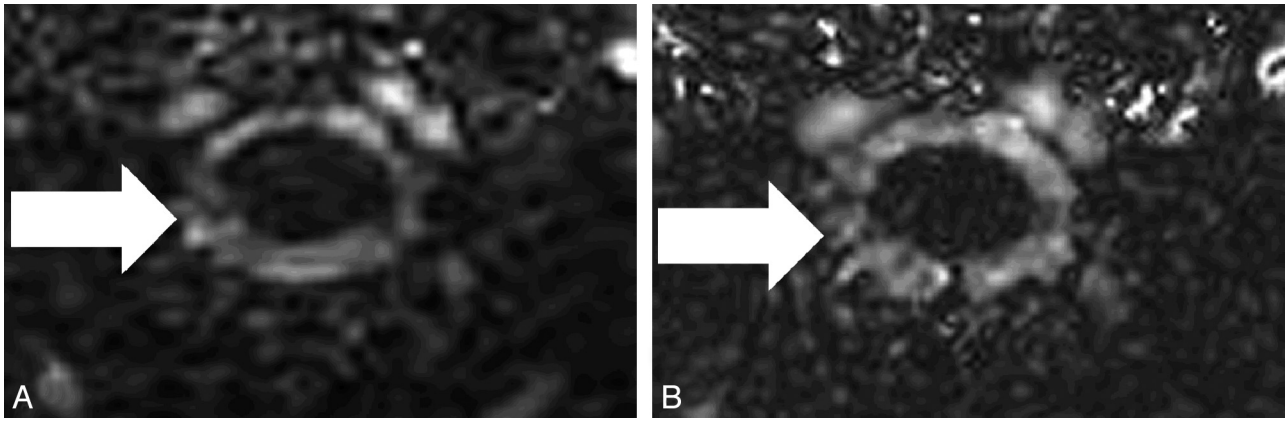

Fig 5. Phase images of CSF acquired at the level of the foramen magnum in 1 healthy volunteer with the CPC (TR/TE = 23.0/6.0 ms) (*A*) and RPC (TR/TE = 14.8/9.2 ms) (*B*) acquisitions. Arrows point to the area of the subarachnoid space at the level of the foramen magnum.

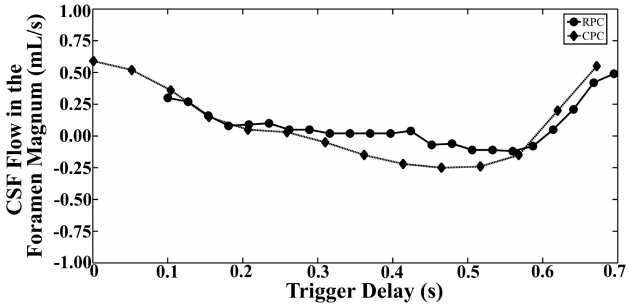

Fig 6. CSF flow over the R-R interval in the foramen magnum of 1 healthy volunteer as measured with the RPC and CPC acquisitions.

Volunteers

Images obtained by using the RPC and CPC acquisitions showed flow in the foramen magnum in both caudad (systole) and cephalad (diastole) directions. Images acquired by using the CPC acquisition showed evidence of poor SNR and ghosting artifacts; images acquired by using the RPC acquisition showed evidence of poor SNR and streak artifacts (Fig 5). However, the streak artifacts did not appear to affect the portion of the image displaying flow in the foramen magnum. Flow measurements calculated from the images showed changes in flow from positive (systole) to negative (diastole) (Fig 6). Peak systolic and diastolic CSF velocities (Table 2) varied from 0.4 to 4.3 cm/s. The average absolute difference between RPC and CPC measurements of peak velocity was 0.2 ± 0.1 cm/s for systolic flow and 0.2 ± 0.2 cm/s for diastolic flow. Peak systolic and diastolic velocities did not differ significantly for the 2 sequences ($P = .85$ and 0.46, respectively).

Table 2: Peak systolic and diastolic CSF velocities in 5 human volunteers at the level of the foramen magnum defined in sagittal images by the tip of the clivus anteriorly and the occipital bone posteriorly

	RPC	CPC	Absolute Difference
Systolic peak velocity (cm/s)			
Volunteer 1	2.2	2.4	0.2
Volunteer 2	4.3	4.0	0.3
Volunteer 3	3.7	3.6	0.1
Volunteer 4	2.1	2.2	0.1
Volunteer 5	2.0	2.2	0.2
Average[a]	2.9 ± 1.1	2.9 ± 0.9	0.2 ± 0.1
Diastolic peak velocity (cm/s)			
Volunteer 1	1.0	1.1	0.1
Volunteer 2	0.9	1.0	0.1
Volunteer 3	1.6	1.4	0.2
Volunteer 4	0.4	0.8	0.4
Volunteer 5	0.8	0.8	0.0
Average[a]	0.9 ± 0.4	1.0 ± 0.3	0.2 ± 0.2

[a] Mean values ± SDs.

Discussion

In this study, for constant laminar flow with average velocities in the range of 0.8–25.3 cm/s, average errors were <11% and 21% and average COVs were 1.29% and 3.01% for the RPC and CPC acquisitions, respectively. For the measurement of peak velocities >12.6 cm/s, the RPC and CPC acquisitions had similar error (~ −35%) and COVs (average = 35.1% and 18.6%, respectively). For peak velocities of ≤12.6 cm/s, the acquisition methods significantly overestimated velocities and had reduced reproducibility. Measurements of CSF velocities in human volunteers and of sinusoidally fluctuating phantom velocities did not differ significantly between the 2 techniques.

PCMR techniques may be used in the evaluation of patients with a Chiari I malformation to determine which patients may benefit from cranio-occipital decompression. In this application, obstructed CSF flow must be distinguished from normal CSF flow. Normal flow patterns tend to be more homogeneous through the subarachnoid space, and normal peak CSF velocities tend to be <4 cm/s.[16] In patients with symptomatic Chiari I, CSF flow tends to be less homogeneous than that in healthy subjects and peak velocities tend to be >4 cm/s.[10] The average CSF velocities found in healthy subjects, patients with asymptomatic Chiari I, and those with symptomatic Chiari I can be measured with a sufficient amount of accuracy and reproducibility with both the RPC and CPC acquisitions. However, peak CSF velocities in healthy subjects and patients with Chiari I differ by a larger amount.[18] Elevated peak velocities, in the range of 12 cm/s, can be measured accurately, but slower peak velocities typical of healthy subjects may not be measured accurately or precisely.

The oscillating CSF flow in the foramen magnum may be measured as average flow in centimeters per second throughout the cardiac cycle. Average flow is determined by the change in brain volume during systole and diastole and presumably does not measure the effect of tonsillar ectopia on

flow. Because the volume of CSF flowing out of the cranial vault during systole equals the amount returning during diastole, CSF stroke volume is zero. Peak velocity is a measure of the inhomogeneity of flow. Assuming no change in cross-sectional area in the CSF space, the presence of greater peak velocities indicates the presence of larger flow jets. Therefore, peak velocity may be an important measure of the complexity of CSF flow. CSF pressure gradients, shear stresses, and other parameters of CSF flow that may be important for evaluating Chiari I malformation may be obtained from computational flow analysis.[19]

Limitations include the fact that the noise in PCMR techniques, which limits the accuracy of measuring slower blood flow rates,[20] confounded the measurements in our studies, especially for average velocities at the nadir of the sinusoidal flow studies (Fig 4) and for peak velocities. However, the accuracy and reproducibility of the RPC and CPC acquisitions measured in this study compare well with measurements of arterial blood flow.[21] For example, a reported PCMR technique had an accuracy of 13% for rapid sinusoidal flow.[22] The reliability of PCMR for vascular velocity and flow measurements has recently become a topic for investigations.[23] Inaccuracies in PCMR may partially be attributed to the advances in gradient performance that also introduce more eddy currents and phase errors that are not compensated for by the current pre-emphasis systems. These errors are amplified in phase-contrast measurements with low VENC settings, such as in the investigation of CSF flow. In future studies, a correction could be made by placing a static phantom in the scanner, measuring the eddy currents effects, and applying the correction.[24]

Furthermore, actual velocities were not known for the experiments on fluctuating flow. Measurements of fluctuating velocity by the RPC and CPC methods approximated a sinusoidal waveform. However, the nadir velocities should have approached 0 cm/s. The inability of the RPC and CPC acquisitions to accurately demonstrate these velocities is possibly due to dampening of the sinusoidal waveform over the length of the tubing or the inaccuracy of the flow measurements themselves due to noise and the effects of eddy currents. Finally, flow in the tubing does not reproduce the complex anatomy of the subarachnoid space, the complex flow patterns in vivo, or the physiologic movement of the borders of the fluid space. However, the magnitude of error measured in these experiments is likely to estimate the errors in clinical studies to measure average and peak velocities.

In future studies it may be useful to compare the peak velocities of CSF as measured with the RPC and CPC methods in healthy subjects and in subjects with a Chiari I malformation. Such a prospective study would elucidate the ability of these methods to distinguish healthy subjects from subjects with a Chiari I malformation. Additionally, newer methods of improving the SNR need to be developed and used with these PCMR techniques to improve the accuracy and precision at the lowest velocities studied above.

Conclusions

The RPC and CPC sequences measure velocities on the order of CSF flow with an average error of ≥9%. These techniques overestimate peak velocities <6.4 cm/s. Measurements of CSF velocities in human volunteers and of sinusoidally fluctuating phantom velocities did not differ significantly between the 2 techniques.

Acknowledgments

We thank Kelli Hellenbrand for her help in scanning volunteers and Jason Fine for his assistance with the statistical analysis.

References

1. Lotz J, Meier C, Leppert A, et al. **Cardiovascular flow measurement with phase-contrast MR imaging: basic facts and implementation.** *Radiographics* 2002;22:651–71
2. Edelman RR, Wedeen VJ, Davis KR, et al. **Multiphasic MR imaging: a new method for direct imaging of pulsatile CSF flow.** *Radiology* 1986;161:779–83
3. Levy LM, Di Chiro G. **MR phase imaging and cerebrospinal fluid flow in the head and spine.** *Neuroradiology* 1990;32:399–406
4. Enzmann DR, Pelc NJ. **Normal flow patterns of intracranial and spinal cerebrospinal fluid defined with phase-contrast cine MR imaging.** *Radiology* 1991;178:467–74
5. Feinberg DA, Mark AS. **Human brain motion and cerebrospinal fluid circulation demonstrated with MR velocity imaging.** *Radiology* 1987;163:793–99
6. Levy LM. **MR identification of Chiari pathophysiology by using spatial and temporal CSF flow indices and implications for syringomyelia.** *AJNR Am J Neuroradiol* 2003;24:165–66
7. Levy LM. **Toward an understanding of syringomyelia: MR imaging of CSF flow and neuraxis motion.** *AJNR Am J Neuroradiol* 2000;21:45–46
8. Heiss JD, Patronas N, DeVroom HL, et al. **Elucidating the pathophysiology of syringomyelia.** *J Neurosurg* 1999;91:553–62
9. Barger AV, Peters DC, Block WF, et al. **Phase-contrast with interleaved undersampled projections.** *Magn Reson Med* 2000;43:503–09
10. Haughton VM, Korosec FR, Medow JE, et al. **Peak systolic and diastolic CSF velocity in the foramen magnum in adult patients with Chiari I malformations and in normal control participants.** *AJNR Am J Neuroradiol* 2003;24:169–76
11. Foo TK, Bernstein MA, Aisen AM, et al. **Improved ejection fraction and flow velocity estimates with use of view sharing and uniform repetition time excitation with fast cardiac techniques.** *Radiology* 1995;195:471–78
12. Greil G, Geva T, Maier SE, et al. **Effect of acquisition parameters on the accuracy of velocity encoded cine magnetic resonance imaging blood flow measurements.** *J Magn Reson Imaging* 2002;15:47–54
13. Stahlberg F, Mogelvang J, Thomsen C, et al. **A method for MR quantification of flow velocities in blood and CSF using interleaved gradient-echo pulse sequences.** *Magn Reson Imaging* 1989;7:655–67
14. Ohara S, Nagai H, Matsumoto T, et al. **MR imaging of CSF pulsatory flow and its relation to intracranial pressure.** *J Neurosurg* 1988;69:675–82
15. Wentland AL, Korosec FR, Vigen KK, et al. **Cine flow measurements using phase contrast with undersampled projections: in vitro validation and preliminary results in vivo.** *J Magn Reson Imaging* 2006;24:945–51
16. Quigley MF, Iskandar B, Quigley ME, et al. **Cerebrospinal fluid flow in foramen magnum: temporal and spatial patterns at MR imaging in volunteers and in patients with Chiari I malformation.** *Radiology* 2004;232:229–36
17. Berger SA, Talbot L, Yao LS. **Flow in curved pipes.** *Annu Rev of Fluid Mechanics* 1983;15:461–512
18. Dolar MT, Haughton VM, Iskandar BJ, et al. **Effect of craniocervical decompression on peak CSF velocities in symptomatic patients with Chiari I malformation.** *AJNR Am J Neuroradiol* 2004;25:142–45
19. Roldan A, Wieben O, Haughton V, et al. **Characterization of CSF hydrodynamics in the presence and absence of tonsillar ectopia by means of computational flow analysis.** *AJNR Am J Neuroradiol* 2009;30:941–46
20. Lee VS, Spritzer CE, Carroll BA, et al. **Flow quantification using fast cine phase-contrast MR imaging, conventional cine phase-contrast MR imaging, and Doppler sonography: in vitro and in vivo validation.** *AJR Am J Roentgenol* 1997;169:1125–31
21. McCauley TR, Pena CS, Holland CK, et al. **Validation of volume flow measurements with cine phase-contrast MR imaging for peripheral arterial waveforms**. *J Magn Reson Imaging* 1995;5:663–68
22. Robertson MB, Kohler U, Hoskins PR, et al. **Quantitative analysis of PCMRI velocity maps: pulsatile flow in cylindrical vessels.** *Magn Reson Imaging* 2001;19:685–95
23. Gatehouse PD, Rolf MP, Graves MJ, et al. **Evidence across CMR sites and systems of phase-contrast background velocity offsets requiring correction for accurate regurgitant or shunt flow.** In: *Proceedings of the 17th International Society for Magnetic Resonance in Medicine*, Honolulu, Hawaii; April 18–24, 2009
24. Caprihan A, Griffey RH, Fukushima E. **Velocity imaging of slow coherent flows using stimulated echoes.** *Magn Reson Med* 1990;15:327–33